International Journal of Hydrogen Energy 206 (2026) 153393

Contents lists available at ScienceDirect

International Journal of Hydrogen Energy

journal homepage: www.elsevier.com/locate/he

Directly electrified SiSiC packed foam reactor for methane steam reforming: experimental study and model-based scaleup

Federico Nicolini, Matteo Ambrosetti, Alessandra Beretta, Gianpiero Groppi *, Enrico Tronconi

Laboratory of Catalysis and Catalytic Processes, Dipartimento di Energia, Politecnico di Milano, 20156, Milano, Italy

ARTICLE INFO

Keywords:
Electrified reactors
Steam methane reforming
Hydrogen production
Structured catalysts
Process intensification

ABSTRACT

The interest in hydrogen production is higher than ever due to its key role as carbon-free energy carrier. In this work we propose a concept of electrified Steam Methane Reforming (e-SMR) reactor where a directly Joule-heated silicon infiltrated silicon carbide (SiSiC) foam provides heat to catalytic pellets packed inside the foam openings. All the advantages associated with a pelletized catalyst are maintained while a close coupling of heat generation by the foam with heat consumption by the catalytic reaction is guaranteed. An experimental campaign demonstrated the intensification potential of the reactor, which achieved specific power inputs up to 10 MW/m^3 and specific energy consumptions of 1.33 kWh/Nm$^3_{H2}$.

A 2-D heterogeneous mathematical model was validated against the experimental data while a strategy based on sectioning the foam into several slices electrically connected in series is proposed to meet the requirements of low pressure drops and high electric circuit resistances necessary in scaled up units.

List of symbols

Symbol	u.o.m.	meaning
ε	[−]	Porosity of packed bed
V	$[m^3]$	Pellet volume
λ	$[Ncc/min]$	Extent of reaction
r	$[m]$	radius
F_i	$[Ncc/min]$	volumetric flow rate referred to the ith specie
$\dot{H}$	$[J/s]$	Enthalpy flux
P_{el}	$[W/m^3]$	Electric power
ΔH	[J/mol]	Heat of reaction
v	$[m/s]$	Gas velocity
C_i	$[mol/m^3]$	Concentration of the ith specie
D_i	$[m^2/s]$	Diffusivity of the ith specie
$\nu_{i,j}$	[−]	Stoichiometric coefficient of the ith species referred to the jth reaction
rr_j	$[mol/(g_{cat}\cdot s)]$	Reaction rate of the jth reaction
G	$[kg/(m^2\cdot s)]$	Mass flow rate
cp	$[J/(kg\cdot K)]$	Specific heat
T	$[K]$	Temperature
k	$[W/(m\cdot K)]$	Thermal conductivity
h_v	$[W/(m^2\cdot K)]$	Heat transfer coefficient between solid phase and pseudophase
P	$[Pa]$	Pressure

(*continued on next column*)

(*continued*)

Symbol	u.o.m.	meaning
Sv_{tot}	$[m^{-1}]$	Total specific surface area
μ	$[Pa\cdot s]$	Dynamic viscosity
ρ	$[kg/m^3]$	density
U	$[W/(m^2\cdot K)]$	Overall heat transfer coefficient
h_w	$[W/(m^2\cdot K)]$	Heat transfer coefficient between the inner wall of the reactor and one of the two phases
P_i	$[atm]$	Partial pressure of the ith specie
k_j	$[mol/(atm\cdot g_{cat}\cdot s)]$	Kinetic constant of the jth reaction
$K_{P,j}$	[−]	Reaction ratio of the jth reaction
$K_{EQ,j}$	[−]	Equilibrium constant of the jth reaction
$K_{ads\ i}$	$[atm^{-1}]$	Adsorption constant of the ith reaction
Res	$[m\cdot K/W]$	thermal resistance
ϱ_{el}	$[\Omega\cdot m]$	Electric resistivity
σ	$[A/m^2]$	Current density

Sub/ superscript	meaning
cat	Referred to packed catalyst
$foam$	Referred to the foam
$reactor$	Referred to the reactor, foam + catalyst
in	Reactor Inlet section
out	Reactor outlet section

(*continued on next page*)

* Corresponding author.
E-mail address: gianpiero.groppi@polimi.it (G. Groppi).

https://doi.org/10.1016/j.ijhydene.2026.153393
Received 3 November 2025; Received in revised form 23 December 2025; Accepted 4 January 2026
Available online 9 January 2026

(*continued*)

Sub/ superscript	meaning
exp	Experimental value
b	Bulk value
PP	Pseudophase
S	Solid phase
wall	reactor wall
eff	Effective value
ax	axial direction
rad	radial direction
ext	external natural convection
ins	insulant layer
eq	Equivalent external resistance, external convection + insulant layer resistance

1. Introduction

The reduction of carbon dioxide emissions has become an imperative in modern society to keep global warming under control [1]. Great efforts are required within the so-called hard-to-abate sectors with chemical industries belonging to this category [2]. Relying on fossil fuels both as feedstock and energy sources, chemical plants are responsible for 5 % of global CO_2 emissions but, due to the vast range of applications, their decarbonization could be one of the keys for achieving net-zero emissions in the forthcoming years [3]. A share of emitted greenhouse gases is related to the production of hydrogen, which is a key reactant in several chemical processes such as methanol and ammonia synthesis [4,5]. In addition to that, hydrogen is also envisioned as an important energy carrier with a promising role as fuel for industries [6,7] and vehicles [8], leading to a growing demand in the forthcoming years. Nowadays, steam methane reforming is the most common and cheapest way of producing hydrogen and syngas but, due to its high endothermicity and presence of carbon in the feedstock, it implies the emission of more than 10 kg CO_2 per kg of H_2 produced, 40 % of which are originated from heat supply by burners [9,10].

$$CH_4 + H_2O \rightleftharpoons CO + 3H_2 \quad \Delta H_r^0 = 206\ kJ/mol \tag{1}$$

$$CO + H_2O \rightleftharpoons CO_2 + H_2 \quad \Delta H_r^0 = -41\ kJ/mol \tag{2}$$

Conventional reformers are constituted by a number of long and slender tubes packed with catalyst pellets. These are placed in a furnace where heat is produced via burners fed with fossil fuels which bring the temperature of the catalytic bed over 900 °C at the exit of the reactor. However, since the packed bed is characterized by poor heat transfer, the radial temperature distribution in this system shows a minimum in the centre of the reactor tubes, which translates into non-optimal working conditions for the catalyst. To mitigate the temperature gradient in the catalytic bed, the tubes must have a small diameter and a high specific surface area which increases the heat transfer rate. To minimise the radial temperature gradient in the catalytic bed and decrease the CO_2 emissions originated from this process, a possible solution consists in implementing structured electrified methane steam reforming reactors such that the heating source shifts from fossil fuels to renewable energy [11]. In literature several different electrification technologies are proposed, which rely on various working principles such as microwave heating, plasma, induction and Joule heating [12–15]. While the first three mechanisms are affected by limited energy efficiencies and issues related to scalability [16], the latter approach can guarantee in principle full conversion of electric energy into heat. Moreover, this concept is suitable for different reactor scales, making it a good candidate for chemical plants that demand flexibility and scalability.

Starting from the pioneering work of Chorkendorff and co-workers [17,18], in recent years several solutions for electrifying chemical reactors have been implemented in laboratories or studied via mathematical models. The group of Balakotaiah [19] proposed the use of resistive heating wires which provided energy to washcoated catalyst highlighting the need of proposing solutions which could be easily scaled up to industrial relevant sizes. The same group also drawn attention on the catalytic activation of electrified reactors, pointing out that the washcoating strategy is often preferred when dealing with Joule-heated electrified reactors. They concluded that, unlike automotive applications where this strategy is already consolidated, in Joule-heated reactors efforts must be done in order to understand the durability of catalyst when directly applied on the resistive element since, in some cases, it could change the resistivity of the support or be subject to deactivation, phenomena which could lead to uncontrolled local hotspots [20] and, therefore, loss of performance. Pashchenko et al. [21] reported a modelling study of a washcoated electrified wire showing that, to achieve full methane conversion, the wire must sustain an operating temperature of 1400 K. This result supports the claims of Balakotaiah et al. who highlighted the issues related to the adhesion of catalytic layers [20] and catalyst stability on supports characterized by different expansion coefficient with respect to the washcoated layer. Rieks et al. [22] examined the performance of a La–Ni–Ru catalyst laid on an electrical resistance in Dry Reforming, a configuration conceived for small-scale application. More recently, Vlachos and co-workers led several studies on the effect that pulsed heating has in Joule-heated reactors [23,24]. Several reactions were tested in different conditions using a reactor constituted of a lightweight and porous resistive carbon paper washcoated with catalyst.

To enable process electrification and intensification at larger scale, the adoption of structured catalysts already proved to be a desirable solution as witnessed by recent patent literature based on monolith catalysts [25,26]. The adoption of these multichannel structures aims at promoting heat and mass transfer properties, allowing the catalyst to be used more efficiently [27,28] while enabling, at the same time, a reduction in the size of the reactors and enabling process intensification [29]. As an alternative, our group proposed the use of open cell foams which, thanks to their open and interconnected 3D structure, guarantee better transport properties if compared to monoliths [30] and avoid flow maldistribution in the catalytic bed, an important aspect which adversely affects monoliths with segregated channels.

An electrified Steam Methane Reforming (e-SMR) concept based on a silicon-infiltrated silicon carbide open cell foam acting both as heating element and support for a rhodium-based catalyst was already proposed by Zheng et al. [31] The performance of a washcoated foam was investigated over a range of gas hourly space velocities (GHSV) and steam to carbon ratios (S/C) for different reactions aiming at hydrogen or syngas production [32]. Thanks to the intimate contact of the heating source with the catalyst and the remarkable heat and mass transfer properties of the foam, this concept proved to guarantee excellent performance in terms of methane conversion and energy consumption, achieving full methane conversion with specific energy consumptions remarkably lower than in electrolyzers [31,33]. Moreover, as described by Song et al. who modelled this kind of system [34], the uniform heat generation in the catalytic bed allows for flat radial temperature profiles.

In all the studies presented so far, catalytic activity was brought to the by washcoating techniques. Attempts of electrification of packed beds were done by Zheng et al. [35], who led experiments on a small lab scale Joule heated SiSiC foam filled with powder dry reforming catalyst. An alternative solution was proposed by Lu and Nikrityuk [36,37], whose experimental and modelling activity described a tube packed with catalyst particles mixed with electrically conductive spheres which, when contacting each other, acted as an electrical circuit and generated heat via Joule effect, an approach also investigated by Turan et al. [38]. Authors showcased the possibility of this concept of being scaled up, providing a solution for the electrification of packed beds. However, they also hinted at limitations on the applicability of this concept for processes where high working temperatures are required due to the thermal expansion of the different materials present in the reactor which

led to variations in the electrical resistance. Another bottleneck is related to the catalyst inventory inside the reactor. Catalyst volume fraction up to 66.6 % (i.e. 33.4 % electrically conductive material) were achieved while maintaining a reasonable electrical conductivity only with bimodal particle size distribution (dcat/dcond>2), which may result in packing uniformity issue when scaling up.

This work proposes for the first time a complete demonstration of the concept of directly electrified SiSiC packed foam reactor. We present experimental evidence, corroborated by mathematical simulations, which emphasizes its relevance at the industrial level by proposing design of scaled up units. To achieve these results, a new lab-scale reactor was engineered to perform experiments while a model describing the interaction between a directly electrified foam and pellet catalyst was implemented in MatLab. Finally, we introduce for the first time a method for realizing a scaled-up version of this system characterized by a low length/diameter aspect ratio, which allows to mitigate pressure drops while ensuring appropriate electrical resistance of the packed foam in the catalytic bed.

2. Materials and methods

2.1. Experimental

2.1.1. Catalytic packed foam

In analogy with previous studies [31,33] where a α-SiSiC foam was used both as catalyst support and heat generation medium, in the present work we used a 10 PPI SiSiC open cell foam 80 mm long with a diameter of 35 mm purchased from EngiCer SA (Table 1).

Acting as an electrical resistance, the foam provided heat to the catalyst. However, differently from what previously proposed by this group, catalytic activity was provided by pellet catalyst instead of washcoating (Fig. 1). To properly pack this foam, small spherical pellets are necessary to avoid catalyst maldistribution that would generate hotspots in the reactor and a consequent decay in performance [39]. Therefore, for this application, Rh-γAl_2O_3 (0.3 % w/w) pellets with a diameter of 1 mm supplied by Heraeus were used (Fig. 1). The size of the pellets must be chosen such that the d_{pore}/d_{pellet} ratio is greater than 2.5 [40], a threshold that ensures a packing density (*3*) of the foam around 0.6, i.e., very close to the packing density of a conventional packed bed:

$$1 - \varepsilon_{packing} = \frac{V_{pellets}}{\varepsilon_{foam}\, V_{react}} \quad 3$$

Despite being an expensive metal, rhodium already demonstrated excellent performance in methane steam reforming and dry reforming conditions [32] in terms of methane conversion activity and resistance against carbon formation. These characteristics make it a sensible choice for intensified applications where small amounts of catalyst are required but high levels of catalytic activity are necessary to sustain high gas hourly space velocities.

In these campaigns, 38 g of pellets have been loaded filling 80 % of the total foam length. Based on a particle density of 1.3 g/cm^3 obtained by packing experiments in empty calibrated cylinders, such a load corresponds to a packing density in the foam voids of 56 %, which matches well the expected one proving the uniform packing of particles in the structure [40]. In analogy to the washcoated setup [33], the remaining 20 % (the entrance zone) was used as a pre-heating section since reactants enter the reactor below 200 °C while methane steam reforming requires higher temperatures.

Table 1
Geometrical properties of the tested SiSiC foam sample.

D [mm]	L [mm]	ε_{foam} [%]	Sv [m^{-1}]	d_{pore} [mm]	d_{cell} [mm]	Bulk resistivity [Ωm]
35	80	80	560	2.5	5	0.0004

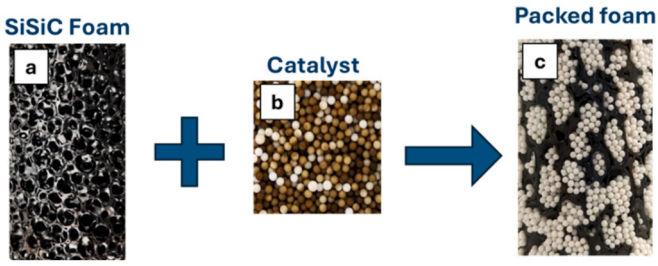

Fig. 1. Packed foam concept: the pores of the SiSiC foam (a) are filled with pellet catalyst (b). The SiSiC element provides heat to the catalyst (c).

2.1.2. Electrified reactor

As illustrated in Fig. 2, the packed foam was tested in a stainless-steel reactor from which was electrically insulated by means of a flanged quartz liner. Because of the pressure drops introduced by the pellet catalyst, this latter component (SI, Fig. S1) was designed to prevent gases from bypassing the catalytic bed, flowing through the gap between the electrical insulator and the steel case originated by the different thermal expansion coefficients between the two materials. To guarantee proper sealing, the reactor's tap was bolted to the case applying a pressure on the quartz flange (Fig. 2). In this way, the quartz flange was clamped in between the metallic case and tap. This technical solution was validated with experiments ran at low GHSV where ~100 % conversion was achieved.

The reactor was connected to an AC power supply with a variable transformer that enables us to adjust the input power by imposing a voltage on the SiSiC foam while the current flowing through it changes according to the electrical resistance of the material. To connect the foam to the external AC power supply, two stainless steel electrodes were pressed on the top and bottom surface of the silicon carbide cylinder, respectively. As illustrated in SI, Fig. S2, the electrodes consisted of a long rod which ends at one side with a flat circular plate characterized by the same diameter as the foam, with holes drilled on it to enable gases to flow through. In between the flat metallic electrodes and the silicon carbide foam, a commercial copper porous felt was placed to ensure a better contact between the components of the circuit and, at the same time, to act as a mechanical filter which kept the pellets well packed in the foam.

Temperature measurements relied on two K-type thermocouples placed at the inlet and outlet of the reactor. While the former was located in the duct at the entrance, the latter was carefully positioned as close as possible to the bottom end of the SiSiC foam. This was done by exploiting the previously mentioned holes located on the electrode where a thermocouple can be inserted [32]. This was a crucial aspect to obtain a reliable outlet temperature measure avoiding underestimations of this key parameter [33].

2.1.3. Reaction tests

Upstream of the reactor, feed gases were dosed via Brooks SLA580 mass flow controllers and a water evaporator coupled with a Brooks Quantim series Coriolis mass flow controller. Reactant and product compositions were measured via an on-line μ-GC (Agilent 990) equipped with Molecular Sieve and Porapack columns placed downstream from a custom-made condenser which prevented water to enter the gas analysis section.

While CH_4, CO_2, CO and H_2 concentrations were determined via chromatographic analysis, the water content was estimated via the extents of reaction (*4*,*5*,*6*) which were computed considering the previously proposed reaction scheme (1,2).

$$\lambda_{SMR} = F^{in}_{CH4} - F^{out}_{CH4} \quad 4$$

$$\lambda_{WGS} = F^{out}_{CO2} \quad 5$$

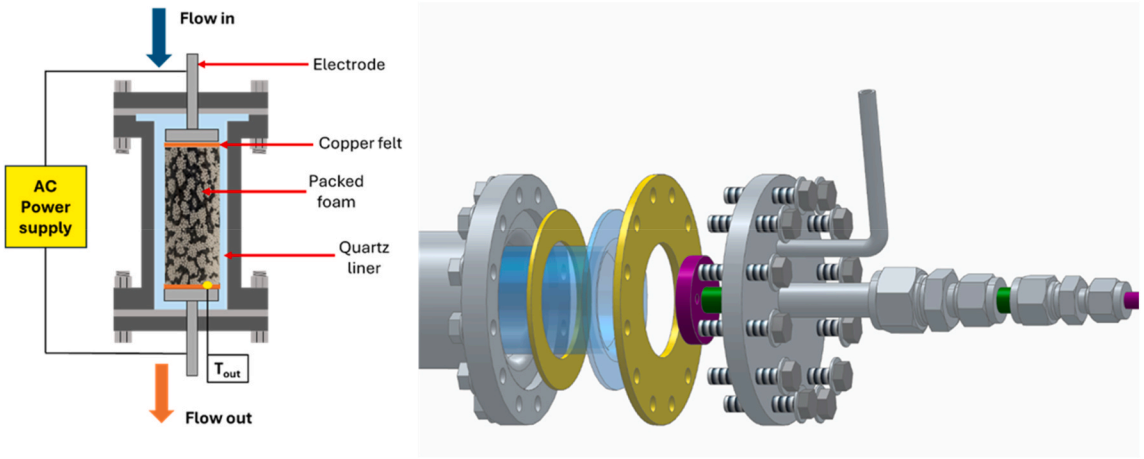

Fig. 2. Reactor scheme and detail of the bypass sealing solution.

$$F_{H2O}^{out} = F_{H2O}^{in} - \lambda_{SMR} - \lambda_{WGS} \quad 6$$

To validate the analysis, the atomic balances were computed as reported in equations (7)–(9), showing a maximum deviation of ± 5 %.

$$C_{bal} = \frac{F_{CH4}^{out} + F_{CO}^{out} + F_{CO2}^{out}}{F_{CH4}^{in}} \quad 7$$

$$O_{bal} = \frac{F_{H2O}^{out} + F_{CO}^{out} + 2 \cdot F_{CO2}^{out}}{F_{H2O}^{in}} \quad 8$$

$$H_{bal} = \frac{4 \cdot F_{CH4}^{out} + 2 \cdot F_{H2O}^{out} + 2 \cdot F_{H2}^{out}}{4 \cdot F_{CH4}^{in} + 2 \cdot F_{H2O}^{in}} \quad 9$$

To demonstrate the potential of this reactor configuration, a set of experiments covering different conditions was carried out. Along the same lines of previous work, the effects of Gas Hourly Space Velocity (GHSV) and S/C were investigated in the range of 5000–15000 NL/kg_{cat}/h and 3–4 mol/mol respectively.

The following key indicators were calculated to assess the system performance.

- methane conversion, defined in equation (10)

$$X_{CH4} = \frac{F_{CH4}^{in} - F_{CH4}^{out}}{F_{CH4}^{in}} \ [\%]; \quad 10$$

- thermal efficiency: it represents the fraction of supplied electric power effectively delivered to the reactor to preheat the reactants and convert them into products, and is defined as the ratio between the enthalpy variation across the reactor and the electrical power supplied to it according to equation (11)

$$th.eff. = \frac{\dot{H}_{out} - \dot{H}_{in}}{P_{el}} \ [\%]; \quad 11$$

- the specific energy consumption determines the amount of energy required to produce a unitary amount of hydrogen: it is an essential parameter when comparing this technology with electrochemical devices, and is computed as the ratio of the supplied electric power to the hydrogen flow rate produced by the reactor:

$$sp.cons. = \frac{\dot{P}_{el.}}{F_{H2}^{out}} \left[\frac{kWh}{Nm_{H2}^3}\right]; \quad 12$$

- the last performance indicator considered in the analysis of the reactor is the hydrogen productivity, i.e. the molar flow of hydrogen produced per unit reactor volume, equation (13)

$$prod. = \frac{F_{H2}}{V_{react}} \left[\frac{Nm_{H2}^3}{m_{react}^3 \cdot h}\right]. \quad 13$$

Both the specific energy consumption and the hydrogen productivity were computed assuming the presence of a water gas shift stage downstream of the reforming unit, where the carbon monoxide produced in the electrified reactor is completely converted into CO_2 leading to an increased hydrogen production.

2.2. Mathematical model

In parallel to the experimental activity, a 2D-heterogeneous mathematical model of the packed foam e-SMR reactor was developed in MATLAB to enable a model-based scale up activity.

2.2.1. Model equations

The model consists of a set of mass, energy and momentum balance equations necessary to predict composition, temperature and pressure drops, respectively. Two phases have been considered: a solid phase corresponding to the SiSiC heating element and a pseudo-phase comprising the flowing gas and the catalyst particles. Pellets and gas were lumped into a unique phase since the specific surface (Sv) of the pellets is much higher than that of the foam [41]. In fact, for the 1 mm pellets, this parameter turned out to be around 3000 m^{-1}, i.e. several times bigger than the specific surface of the foam reported in Table 1, which allows to neglect temperature gradients present in between pellet and gas with respect to those in between foam and gas.

For each species, a differential mass balance equation is implemented for the pseudo-phase (14)

$$\frac{\partial(v \cdot C_i)}{\partial z} = \frac{\partial\left(D_{i,ax} \cdot \frac{\partial C_i}{\partial z}\right)}{\partial z} + \frac{1}{r} \cdot \frac{\partial\left(D_{i,rad} \cdot r \cdot \frac{\partial C_i}{\partial r}\right)}{\partial r} + \rho_{cat} \cdot \sum_{j=1}^{react.} \nu_{i,j} \cdot rr_j \quad 14$$

$$i = CH_4, H_2O, CO, CO_2, H_2.$$

where rr is the reaction rate expressed in $mol/g_{cat}/s$:

Being an egg-shell catalyst, internal mass transport resistances can be neglected as already demonstrated by the calculations performed by Ferri et al. [41] where the very same catalyst was used under similar operating conditions.

Two energy balance equations describe the temperature profiles of the pseudo-phase (15) and solid phase (16), respectively.

$$G \cdot cp \cdot \frac{\partial T_{PP}}{\partial z} = \frac{\partial\left(k_{PP,ax} \cdot \frac{\partial T_{PP}}{\partial z}\right)}{\partial z} + \frac{1}{r} \cdot \frac{\partial\left(k_{PP,rad} \cdot r \cdot \frac{\partial T_{PP}}{\partial r}\right)}{\partial r} + h_v \cdot (T_s - T_{PP}) - \rho_{cat} \cdot \sum_{j=1}^{react.} \Delta H_{r,j} \cdot rr_j \quad (15)$$

$$k_{S,ax} \cdot \frac{\partial^2 T_S}{\partial z^2} + k_{S,rad} \cdot \frac{1}{r} \cdot \frac{\partial\left(r \cdot \frac{\partial T_s}{\partial r}\right)}{\partial r} + h_v \cdot (T_{PP} - T_s) + \varrho_{eff,el} \cdot \sigma^2 = 0 \quad (16)$$

Equation (15) accounts for convection, conduction and heat exchange between the solid phase and the pseudo phase, as well as for the reaction heat consumption. Equation (16) includes terms related to axial and radial conductivity, heat transfer between phases and the Joule heating energy generation term obtained as the product between resistivity $(\varrho_{eff,el})$ and the square of the current density σ, which was taken as uniform assuming a homogeneous structure of the foam and an ideal current distribution by perfect contact with the electrodes.

Pressure drops across the catalytic bed are computed by the modified Ergun expression for packed foams (17) proposed by Ambrosetti et al. [40]:

$$\frac{dP}{dz} = -\left(4.17 \cdot Sv_{tot}{}^2 / \varepsilon_{tot}{}^3 \cdot \mu \cdot v + 0.292 \cdot Sv_{tot} / \varepsilon_{tot}{}^3 \cdot \rho_{gas} \cdot v^2\right) \left[\frac{Pa}{m}\right] \quad (17)$$

where ε_{tot} is obtained as the product of the packed bed porosity and the foam porosity and the total specific surface area as $Sv_{tot} = Sv_{foam} + Sv_{packing}$.

This system of equations is accompanied by a set of boundary conditions reported in Table 2.

At the inlet of the reactor, temperature and gas composition are assigned to the gas phase while an adiabatic condition was assigned to the solid phase [25]. A null temperature derivative was also imposed at the outlet of the reactor for both energy balances. Radial boundary conditions in proximity of the outer radius (equations 21, 22) were implemented to describe thermal losses across the external reactor wall. The sum of the pseudo-phase and solid phase heat fluxes from the wall to the ambient was instead described by equation (31), which allowed to determine the wall temperature T_{wall}.

$$q_{eq} = h_{w,PP} \cdot [T_{wall} - T_{PP}] + h_{w,S} \cdot [T_{wall} - T_S] = U_{eq} \cdot [T_{amb} - T_{wall}] \quad (31)$$

In the centre of the reactor ($r = 0$), a zero-gradient condition for both energy equations was implemented due to symmetry reasons. Regarding the momentum balance, the outlet pressure P was set as a boundary condition.

Table 2
Boundary conditions implemented in the 2D heterogeneous model.

Domain	Boundary condition	
$z = z_{in}$	$T_{PP} = T_{in,exp}$	18
$z = z_{in}$	$\frac{\partial T_S}{\partial z} = 0$	19
$z = z_{in}$	$C_{i,in} = C_{in,exp}$	20
$r = R_{ext}$	$k_{rad\ PP} \cdot \frac{\partial T_{PP}}{\partial r} = h_{w,PP} \cdot [T_{wall} - T_{PP}]$	21
$r = R_{ext}$	$k_{eff(rad)} \cdot \frac{\partial T_S}{\partial r} = h_{w,S} \cdot [T_{wall} - T_S]$	22
$r = R_{ext}$	$\frac{\partial C_i}{\partial r} = 0$	23
$r = 0$	$\frac{\partial T_{PP}}{\partial r} = 0$	24
$r = 0$	$\frac{\partial T_S}{\partial r} = 0$	25
$r = 0$	$\frac{\partial C_i}{\partial r} = 0$	26
$z = z_{out}$	$\frac{\partial T_{PP}}{\partial z} = 0$	27
$z = z_{out}$	$\frac{\partial T_S}{\partial z} = 0$	28
$z = z_{out}$	$\frac{\partial C_i}{\partial z} = 0$	29
$z = z_{out}$	$P = P_{out,exp}$	30

2.2.2. Model parameters

The following reaction rate equations were taken from the work of Ambrosetti et al. [42] and Ferri et al. [41],

$$rr_{SMR} = 0.4 \cdot \frac{kr_{SMR}\ P_{CH4}\ \left(1 - K_{P,SMR}/K_{EQ,SMR}\right)}{1 + K_{adsCO}\ P_{CO}} \left[\frac{mol}{g_{cat}\ s}\right] \quad (32)$$

$$rr_{WGS} = 0.6 \cdot \frac{kr_{WGS}\ P_{H2O}\ P_{CO}}{1 + K_{adsCO}\ P_{CO}}\ \left(1 - K_{P,WGS}\ /\ K_{EQ,WGS}\right) \left[\frac{mol}{g_{cat}\ s}\right] \quad (33)$$

Gas properties were estimated according to the NIST database and mixing rules [43]. Effective gas diffusivities used in the mass balance equations were computed according to Delgado et al. [44].

The effective conductivities of the solid phase in axial and radial directions ($k_{eff(ax)}$, $k_{eff(rad)}$) were equal and computed according to Bracconi et al. [45]

$$k_{eff} = k_b \cdot (1 - \varepsilon_{foam}) \cdot \left(\frac{1}{3} + \frac{2}{3} \cdot (1 - \varepsilon_{foam})\right) \quad (34)$$

The pseudo-phase thermal conductivities (k_{ax}, k_{rad}) were computed according to the correlations proposed by Specchia et al. [46] for packed bed reactors.

The coefficient h_v describes the heat transfer between pseudo-phase and solid phase. As reported by Balzarotti et al. [47], Ambrosetti et al. [48] and Ferri et al. [49], each cell of the foam can be modelled as a pseudo channel having a diameter equal to the cell diameter packed with catalyst pellets. Hence, the coefficients h_w and k_{rad} obtained from Specchia et al. were combined according to the Dixon correlation [50]. In equation (16), the energy generation term that appears in this expression is referred to the electric power $(\varrho_{eff,el} \cdot \sigma^2)$ converted into heat. The electric resistivity $(\varrho_{eff,el})$ of the SiSiC foam was computed according to equation (34) which, despite having been derived for thermal conductivity, can also be applied for the effective electrical conductivity and, consequently, the electrical resistivity [51].

In equation (16), the energy generation term that appears in this expression is referred to the electric power $(\varrho_{eff,el} \cdot \sigma^2)$ converted into heat. The electric resistivity $(\varrho_{eff,el})$ of the SiSiC foam was computed according to equation (35) which is based on the analogy between heat and electricity conduction [51].

$$\varrho_{eff,el} = \frac{\varrho_{b,el}}{(1 - \varepsilon_{foam}) \cdot \left(\frac{1}{3} + \frac{2}{3} \cdot (1 - \varepsilon_{foam})\right)} \quad (35)$$

The overall heat losses towards the internal wall of the reactor were modelled assuming a heat flux coming from the pseudo-phase and solid phase described by the coefficients $(h_{w,PP}, h_{w,S})$ used in equations (*21*, *22*). When related to the pseudo phase, the coefficient $h_{w,PP}$ was obtained from Specchia et al. [46] while, when accounting for the contribution of the solid phase, $h_{w,S}$ was given by Aghaei et al. [52]. The external heat transfer coefficient (U_{eq}) describing the heat transferred from the wall of the reactor towards the external environment was computed according to equation (39) and adopted in equation (31). It was obtained as a series of conductive (Res_{ins}) and convective (Res_{ext}) thermal resistances (equations (36)–(38)), which account for the effect of the 1 cm thick insulation layer and external natural convection respectively. The correlations used for determining the conductive (k_{ins}) and convective (h_{ext}) coefficients were the same used in Ambrosetti et al. [51].

$$Res_{ext} = \frac{1}{2\pi r_{ext} h_{ext}} \quad (36)$$

$$Res_{ins} = \frac{ln(r_{ext}/r_{int})}{2\pi k_{ins}} \quad 37$$

$$Res_{eq} = Res_{ext} + Res_{ins} \quad 38$$

$$U_{eq} = \frac{1}{2\pi r_{ext} Res_{eq}} \quad 39$$

The main dimensions of the reactor used in the mathematical model are reported in Table S1.

2.2.3. Numerical methods

The solution domain has been discretized by equally spaced backward finite differences along the axial coordinate and by orthogonal collocations with symmetrical polynomials along the radial direction. A 41 axial and 4 radial points grid was needed to achieve numerical convergency. The resulting system of algebraic equations comprising mass, energy and momentum balances was then solved using the Fsolve MatLab routine. A Jacobian pattern was introduced to make the inversion of the Jacobian matrix more efficient.

Steady state solution was achieved by means of a numerical continuation strategy with the current density (σ) as a continuation parameter, using the difference between calculated and experimental enthalpy change across the reactor as the objective function. Details are reported in the SI (section S2).

3. Results and discussion

The experimental campaign was aimed at investigating the behavior of the reactor at different GHSV and S/C ratios to i) demonstrate its performance and ii) collect the data necessary for validating the reactor model. In the following paragraphs the effects of GHSV, outlet temperature and S/C will be analyzed. To allow a fair comparison with washcoated systems, methane steam reforming experiments were carried out under comparable working conditions as in a previous work [33], and the results were employed to validate a mathematical model suitable for the design of scaled-up units.

3.1. Effect of GHSV

To assess the effect of the feed flow rate on the reactor performance, three different levels of GHSV were explored in a range of temperature between 600 and 800 °C. Fig. 3 shows how the methane conversion varied in this range of temperatures for different GHSVs, approaching equilibrium line at high temperature for all GHSVs, while exhibiting a progressive deviation at low temperatures and high flow rates. Fig. 4 shows the plot of methane conversion as a function of the electric power input at different GHSVs. Experimental points showed a linear trend

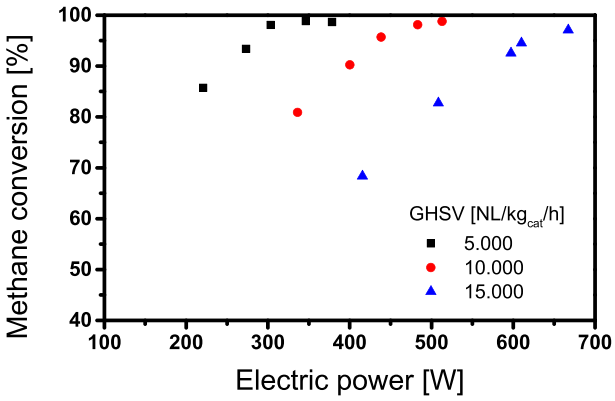

Fig. 4. Methane conversion as function of input power and GHSV. Experiments run at S/C = 4, 1atm and outlet temperature = 600–800 °C.

until full conversion is reached: as expected, higher feed flow rates required a greater amount of power to achieve the same methane conversion. In these conditions 667 W were necessary to convert all the fed methane at 800 °C and 15000 NL/kg$_{cat}$/h, while only 378 W were needed at the lowest GHSV. This trend is in line with our previous studies on washcoated foams and well correlates with the endothermic nature of this reaction.

This range of electric power input corresponds to power densities spanning from 2.9 to 8.7 MW/m^3, a parameter which is useful to assess the intensification potential of reactors. A comparison with the data published by Zheng et al. [33] reveals that packed and washcoated e-SMR reactors reach similar levels of intensification. Even though not pushed to its limits, this system proved to be more power dense than existing full scale industrial methane steam reformers which operate at 7.5 MW/m^3 [53].

Fig. 5 shows that thermal efficiency improves on increasing flow rates, eventually exceeding 70 %. In line with what previously observed in the washcoated foam campaign, this result is ascribed to heat dissipation from the external reactor surface and is strictly related to the high surface to volume ratio of this small-scale experimental setup. In fact, thanks to the close contact between catalyst and heating source, energy can be better transferred to the reaction, enabling efficiencies up to 100 % in a scaled up pseudo-adiabatic reactor. The efficiency trend is reflected in the hydrogen specific energy consumption, which decreases with increasing flow rates. This parameter reflects the amount of energy necessary to produce 1 Nm^3 of hydrogen and enables comparison with electrolyzers under an energetic point of view. Fig. 6 provides a clear picture of the difference between the two technologies. This set of experiments demonstrated that the lab scale rig can achieve specific

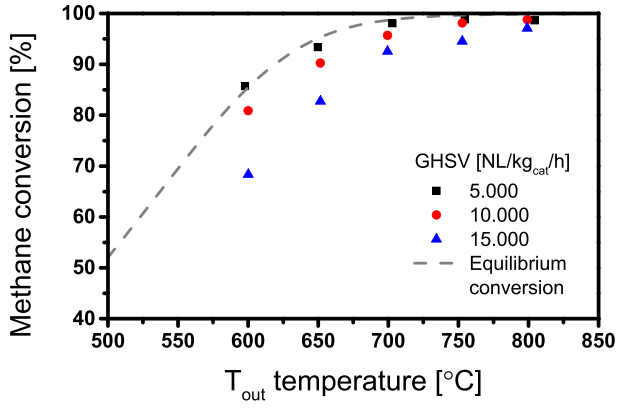

Fig. 3. Effect of GHSV and outlet temperature on methane conversion at S/C = 4 and 1atm.

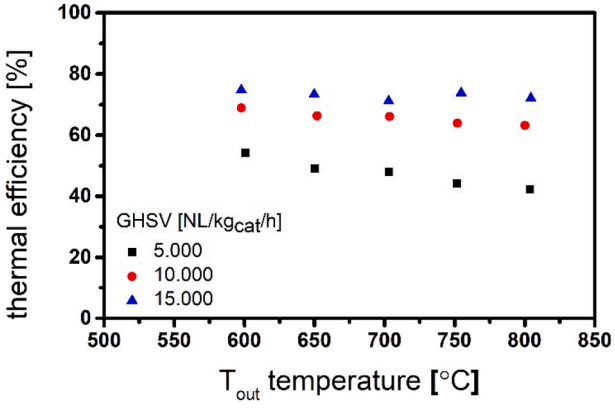

Fig. 5. Effect of GHSV and outlet temperature over thermal efficiency at S/C = 4 and 1atm.

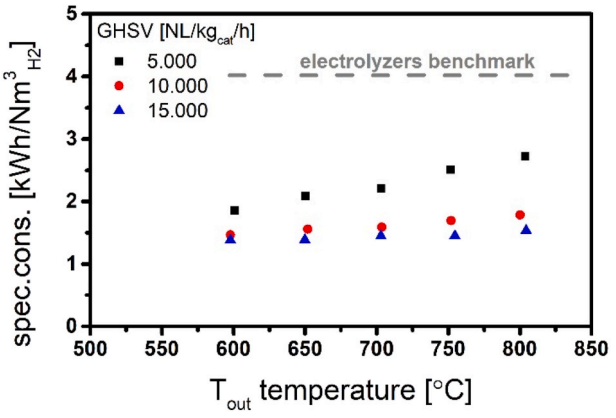

Fig. 6. Effects of GHSV and outlet temperature on the specific energy consumption at S/C = 4 and 1atm.

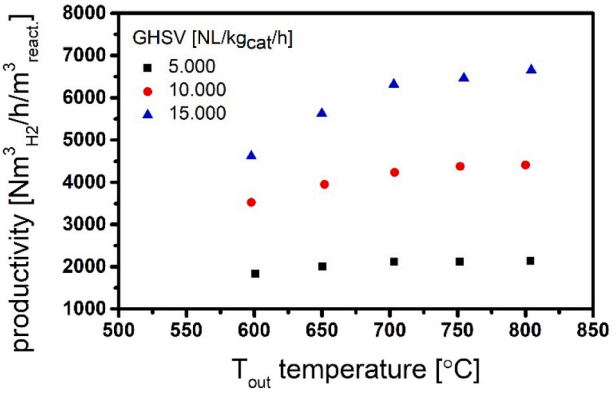

Fig. 7. Effects of GHSV and outlet temperature on H_2 productivity at S/C = 4 and 1atm.

energy demands of 1.4 kWh/Nm$^3_{H2}$, almost one third of what needed by electrolyzers [54] and in line with what observed in the experiments on the washcoated foam [33].

Fig. 7 shows the hydrogen productivity per unit reactor volume. Since the system was able to reach equilibrium at 800 °C at all the tested flow rates, this parameter increased with increasing GHSV since more methane was converted using the same amount of catalyst. In this campaign hydrogen productivities up to 6660 Nm$^3_{H2}$/m$^3_{react}$/h similar to what reported by Zheng et al. [33] for experiments carried out in comparable conditions.

3.2. *Effect of S/C ratio*

Experiments at S/C = 3 and GHSV = 10000 and 15000 NL/kg$_{cat}$/h were also performed. The methane conversion is plotted against the outlet temperature and the electric power in Fig. 8, which shows experimental results collected at different GHSVs. The trend is similar to what was previously described for S/C = 4, exhibiting a reduction of conversion on decreasing temperature and, at temperatures below 750 °C, on increasing GHSV. Like for S/C = 4, the experimental conversion deviated from the equilibrium line below 750 °C due to kinetic effects, a trend that was more pronounced on increasing the flow rate (Fig. S3 in SI). The lower S/C resulted in higher CO concentration in the products (Fig. 8c and Figures S5, S6 in SI) which, according to the kinetic scheme by Ambrosetti et al. [42], was responsible for the lower CH_4 conversion observed at decreasing S/C also in the pure kinetic regime. The higher content of methane in the feed resulted in an increase in the power demand to reach a given conversion (Fig. 8b). In fact, when operating at 15000 NL/kg$_{cat}$/h, 777 W were required to run the system at 800 °C, a substantial increase if compared to the 667 W delivered to the reactor at S/C = 4.

This value translates into a power density of 10 MW/m^3 (computed as described in section 3 of the SI) which is comparable to what already achieved in previous campaigns on washcoated foam [33], confirming that this reactor concept well suits the needs of process intensification.

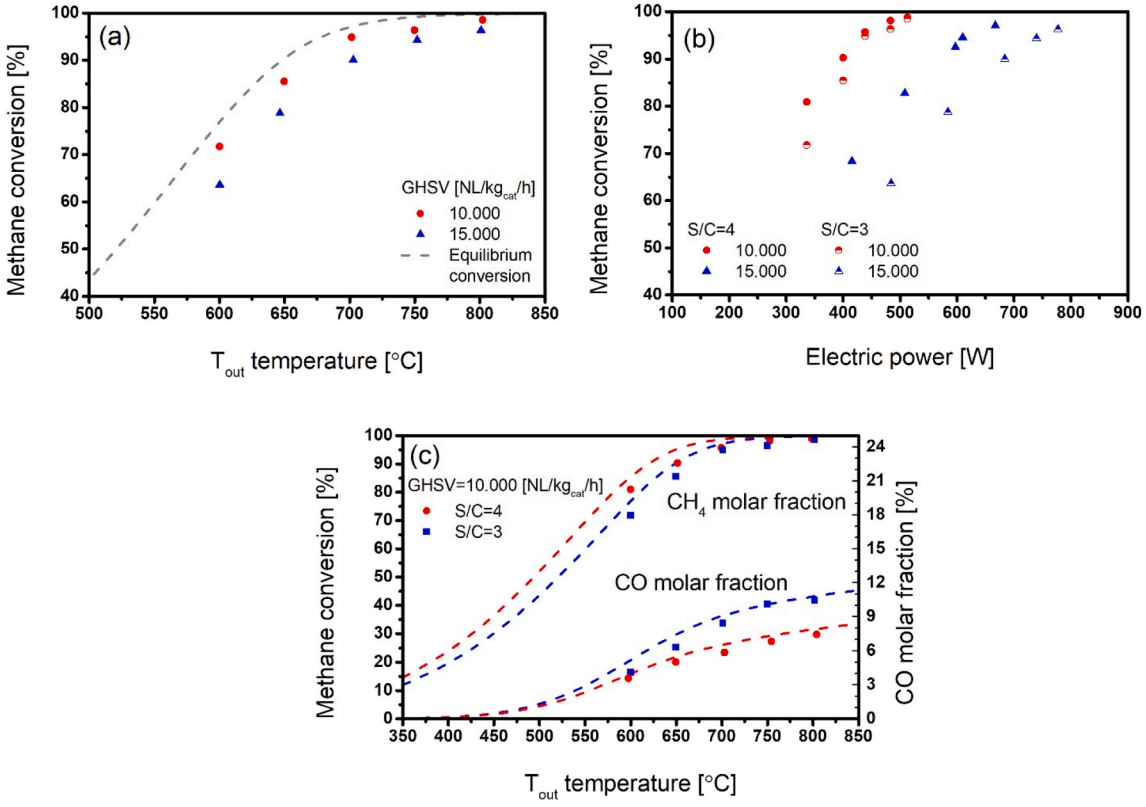

Fig. 8. Effects of GHSV and outlet temperature on methane conversion at S/C = 3 and 1atm. In panels a and c, the dashed lines represent the equilibrium conversion.

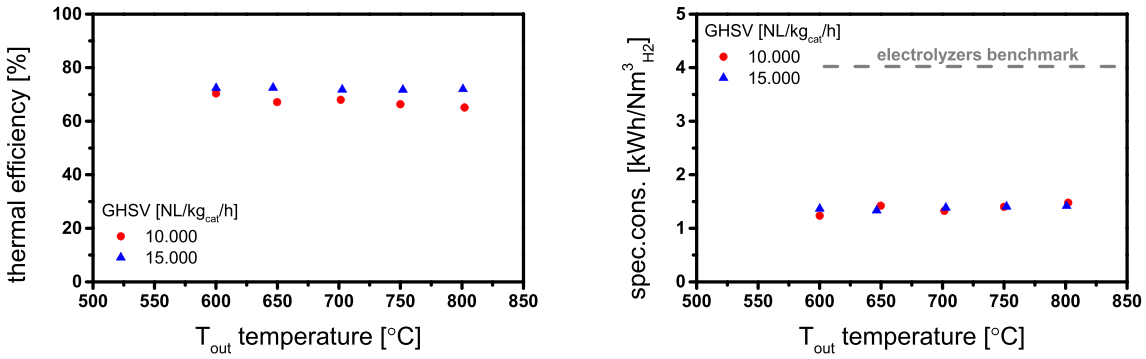

Fig. 9. Thermal efficiency and specific energy consumption at S/C = 3.

As expected, no significant variations were recorded in terms of specific energy consumption or efficiency, following the pattern of the data obtained at S/C = 4.

In line with previous results obtained in a similarly sized washcoated reactor, efficiencies above 70 % and specific energy consumptions down to 1.33 kWh/Nm$^3_{H2}$ were obtained as reported in Fig. 9, corresponding to a specific CO_2 emission of 5.5 kg_{CO2}/kg_{H2} if considering renewable electrical energy. Note that such concentrated CO_2 could be easily captured downstream the WGS reactor by means of PSA resulting in a carbon-free blue hydrogen production.

Despite being already good values for such a small unit, thermal efficiency and specific energy consumption were affected by poor thermal insulation of the lab-scale setup and are expected to improve upon increasing flow rates and reactor size, due to the decreased surface to volume ratio and higher electric power demands. Similar results were obtained by From et al. [55] in an electrified pilot-scale reactor, where experimental efficiencies between 72 and 80 % were measured. Also in this case, the authors showed with the aid of a mathematical model that the system can achieve thermal efficiencies close to 100 % when scaled up.

Finally, it is worth mentioning that the reactor guaranteed stable performance for 30 consecutive hours.

3.3. Model validation

To validate the mathematical e-SMR reactor model, Fig. 10 compares simulated and experimental results. Thermal efficiency, input power (Panel a) and CH_4 conversion (Panel b) are plotted against the outlet temperature for two sets of experiments. Results show that the model predictions can capture with good accuracy the experimental electric power input and, consequently, the measured thermal efficiency and the electric power demand, thus validating the thermal resistance scheme adopted to evaluate heat dissipations.

Similarly, the model, which implements a fully predictive kinetic scheme, faithfully described the experimental methane conversion trend for both the S/C ratios investigated in these campaigns, thus indicating that it captures the temperature evolution along the reactor, including Tout.

A similar accuracy was obtained when comparing simulation results with experiments performed at S/C = 4 with GHSV ranging from 5000 to 15000 NL/kg_{cat}/h as documented in Figs. S4 and S5 of SI.

Calculated axial profiles of temperature and concentrations allow to better elucidate the electrified reactor behaviour. Fig. 11 shows the calculated profiles of the lab-scale reactor when operated at GHSV = 10000 NL/kg_{cat}/h with S/C = 4 and T_{out} = 800 °C.

Simulations showed that CH_4 is completely converted well before the reactor exit, evidencing that this system can handle much higher flow rates while still guaranteeing high levels of conversion, meaning that the investigated conditions are far from the limits of the reactor, which allows for further intensification.

Temperature profiles also provided information regarding the behavior of the preheating zone. In fact, the gas temperature sharply increased in the first section where the catalyst was not packed. In this section, all the power input went into sensible heat, bringing the feed temperature well above 400 °C at the entrance of the catalytic bed. As the reaction proceeded, methane concentration decreased leading to a lower energy demand from the reaction. In this condition, the heating element managed to provide enough energy to increase the temperature of the catalytic bed up to the outlet temperature. This is further highlighted by the sharp temperature increase that occurred in the final section of the reactor where methane was not present anymore, and all the energy supplied in this section heated up the products. A close analysis of this portion revealed a slight reduction of CO_2 concentration, which may be related to the occurrence of the reverse water gas shift. In fact, this reaction is thermodynamically favoured at high temperatures and converts carbon dioxide into CO. Radial temperature profiles reported in SI, Fig. S7 describe the effect of thermal losses on the temperature distribution along the radial coordinate of the lab-scale reactor.

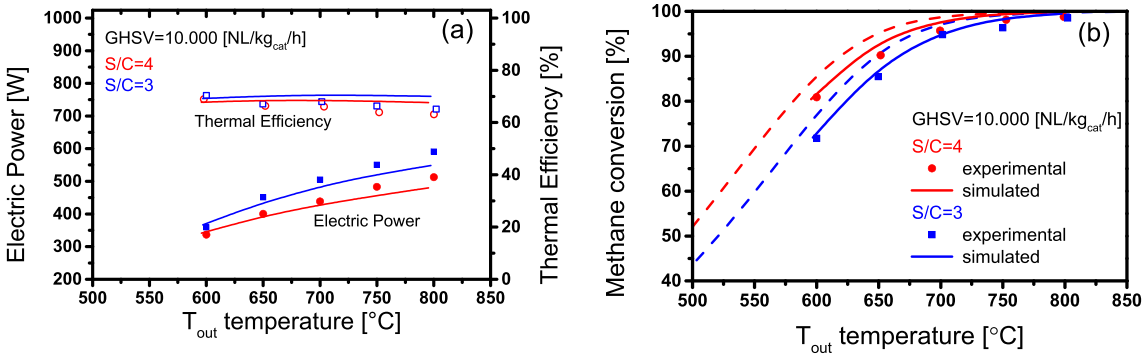

Fig. 10. Model results (lines) versus experimental data (symbols) for GHSV = 10000 NL/kg_{cat}/h and S/C = 4.

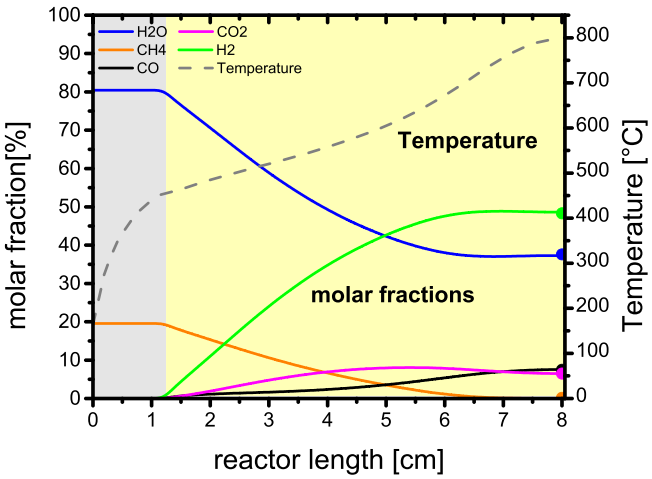

Fig. 11. Simulated composition and pseudo-phase temperature axial profiles of the lab-scale reactor obtained for GHSV = 10000 NL/kg_{cat}/h, S/C = 4 and Tout = 800 °C.

It is apparent that heat losses were more pronounced towards the end of the reactor where higher temperatures were measured.

3.4. Scale-up by mathematical modelling

The validated eSMR reactor model was employed to design scaled-up units aimed at hydrogen or syngas production for different applications. Given the flexibility and scalability of this technology, two different case studies were considered to cover different scenarios. Case A refers to a unit with a target production of 200 Nm^3_{H2}/h, which corresponds to the hydrogen production of a 1 MW electrolyzer. This scenario was modelled to establish a comparison with previous work [33] where a scaled-up washcoated reactor was sized for a small-scale application to be employed in a biogas plant. Differently from lab-scale simulations, an inlet temperature of 500 °C was set as a realistic value of upstream pre-treatment and pre-reforming units [56], while the outlet pressure was set at 8 bar to cope with the requirements of a downstream pressure swing adsorption unit for hydrogen purification, in line with small scale units proposed by Hygear [57]. Finally, a limit on the total pressure drop across the reactor was set at 1 bar and a target voltage-current couple of 380V-650A was identified in accordance to the nominal values of available industrial plugs and to a low voltage grid. To guarantee the hydrogen productivity, a 20 L reactor is necessary when running the system at GHSV = 22500 NL/kg_{cat}/h ensuring equilibrium methane conversion. This value of GHSV was chosen to guarantee the same volumetric flow rate as in the previous work with washcoated foams [33], thus maintaining the same hydrogen productivity per unit reactor volume. To define the aspect ratio of the reactor, the constraints regarding pressure drop and maximum voltage-current are of primary importance. These are indeed conflicting requirements because the former calls for short and wide reactors, while the latter demands slender reactors that maximize the electrical resistance. When adopting a standard configuration as proposed in previous work [33] and in these campaigns with a single cylindrical cellular structure, a foam measuring 1.75 m long and 0.12 m in diameter would be necessary to comply with the voltage-current limitations (380V-650A). However, while this design was well suited to a washcoated foam, a packed foam reactor with pellets of 1 mm diameter would generate 8 bar of pressure drops, definitely a too high value that does not comply with the design requirements. To overcome this limitation, the reactor must be shortened and enlarged to decrease the catalyst bed height and decrease the flow velocity. However, by keeping the same foam specifications, this would imply a dramatic reduction of electric resistance of the foam, resulting in huge currents flowing through the electric circuit. In particular, a foam 0.44 m long with a diameter of 0.24 m would be characterized by an electric resistance of only 0.03 Ω, which would result in a voltage of 85 V and an electric current of 2526 A. To manage this issue, foam sectioning can be implemented to increase the total resistance of the electric circuit while keeping a short and wide reactor design. The cylindrical SiSiC element can be divided into several equal slices electrically connected in series, so that the electric circuit results in a path with increased length and decreased cross-sectional area. Fig. 12 proposes sectioning of the foam into two or four slices, each solution ensuring the same reactor volume while decreasing the pressure drops and keeping the electric resistance unchanged.

Electrical connections could be realised, for example, by alternatively contacting the top and bottom faces of two contiguous slices to form an electrical circuit as illustrated in Fig. 13.

This expedient allows to decouple the aspect ratio of the reactor from the limitations on voltage and current, introducing an important degree of freedom in the system design. Therefore, it is possible to engineer reactors where the electric current flows through a narrower and longer path with respect to the gases which still flow from top to bottom across the whole volume of the catalyst bed. The adoption of such a low length/diameter ratio, which is not allowed in externally heated conventional reform tubes, was made possible thanks to flat radial temperature profiles guaranteed by the uniformly distributed volumetric heating. In this case we halved or divided by four the initial length of the foam and increased the overall diameter by keeping the same total volume.

The porous SiSiC cellular structure can be further sectioned into four equivalent slices (Fig. 12) which, when assembled, results in a reactor with a diameter of 0.24 m and 0.44 m long. Simulation results showed that this setup guarantees the same current-voltage couple as the original design but with a pressure drop of 0.3 bar, definitely lower than the standard configuration as reported in Table 3. Despite the different current path, the previously developed model is valid also for this configuration since the current density remains constant in the whole section as in the standard case. Since the direction of the current through a cross-sectional area do not affect the power generation via Joule effect and the resistivity is the same in the whole domain, a sectioned foam can be modelled as a single foam with hydraulic diameter and length. The electric resistance can then be computed considering the number of slices, therefore increasing the length and reducing the cross-sectional area of the electric circuit.

Another case study (Case B) analyzed in this work aimed at designing a methane steam reforming unit suited for big scale applications, such as oil refineries, methanol or ammonia synthesis plants. In this context, a hydrogen production in the range of 30000–200000 Nm^3/h at 25 bar is required according to the size of the plant. This target can be achieved by combining scaling up with numbering, i.e. with several compact reactors working in parallel. This modular design was based on single reformers with nominal electric power demand of 2 MW. Following the strategy previously described cylindrical reactors with a low length/diameter ratio can be built by sectioning the SiSiC foam in several slices. For this production target, a reactor 1 m long with a diameter of 0.65 m (Fig. 14) is able to produce 1718 Nm^3/h of hydrogen at 25 bar considering inlet and outlet temperatures of 500 and 900 °C. This aspect ratio, combined with a conservative GHSV of 12000 NL/kg_{cat}/h, guarantees a pressure drop within the limit of 1 bar and methane conversion of 88.6 % (Case B, Table 3). This can be obtained by dividing the SiSiC foam into 10 slices which, if connected in series, would ensure an electrical resistance of 1.4 Ω, a value that enables to power the electrified reformer with 1.68 kV and 1.2 kA. The adoption of an almost square aspect ratio can take advantage by the fact that, unlike monoliths, open cell foams do not suffer from issues of flow segregation that would lead to a maldistribution of the reactants in the catalytic beds. It is worth mentioning that the outlet temperature has been chosen due to an operational limit of the Rh catalyst, not of the reactor itself. In fact, unlike traditional reformers where the metallic case reaches high temperature because of their direct exposure to the burners, here it is possible to thermally

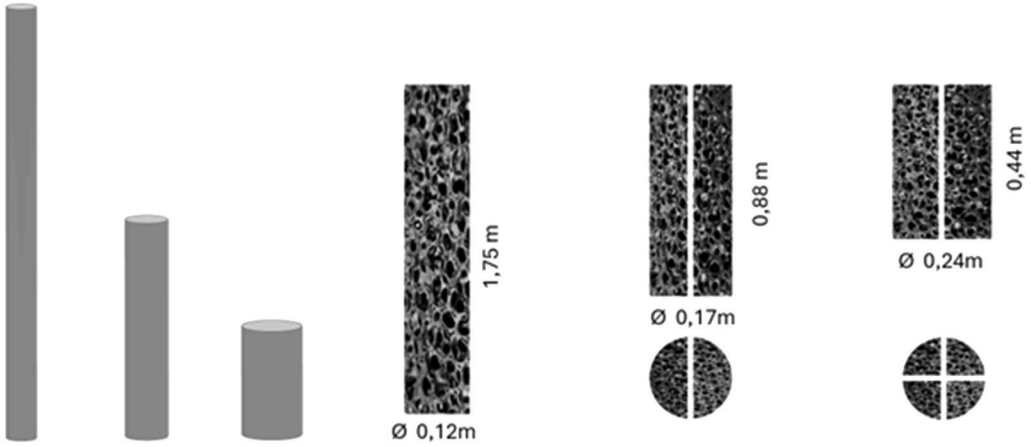

Fig. 12. Reactor configuration for a target production of 200 Nm^3/h (Case A), the picture represents the aspect ratio of the SiSiC foam.

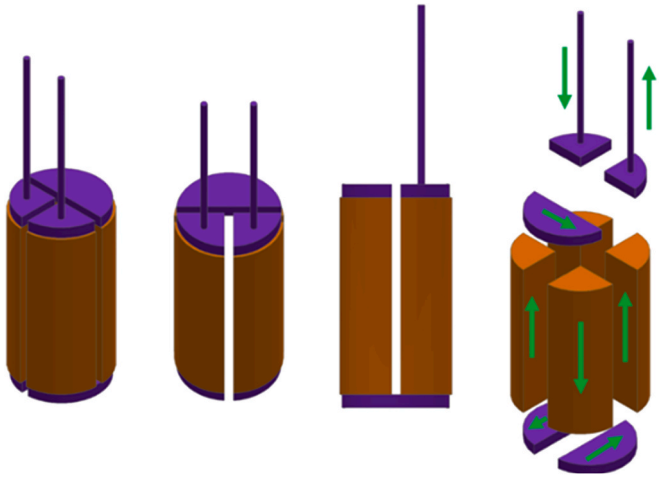

Fig. 13. The picture shows different views of a possible schematic representation of the scaled-up version of the packed foam reactor (reactor case A height = 0.44 m, diam. = 0.24 m). The four slices (orange items) are connected via electrical connections (violet) to form an in-series electrical circuit. Green arrows indicate the path followed by the electric current. Electrical connections must be porous to let the gas flow through along the axial direction. (For interpretation of the references to colour in this figure legend, the reader is referred to the Web version of this article.)

insulate the SiSiC packed foam from the pressure vessel such that its temperature can be kept lower than the catalytic bed one. If combining this aspect with the adoption of a catalyst able to withstand higher temperatures than Rhodium, it is then possible to operate the system at higher pressures and push the methane conversion to approach 100 %.

To establish a comparison with other technologies, configuration B) operates with a power density of 6 MW/m^3, higher than the electrified large scale packed bed modelled by Lu et al. [37] which, according to their simulated results, achieves a value of 2.8 MW/m^3. A specific energy consumption close to 1 kWh/Nm^3_{H2} was predicted in both cases, confirming the capability of this kind of systems to operate with higher efficiencies when scaled up.

4. Conclusions

In this work we provide an experimental and modelling study of a Joule heated packed foam reactor. A directly electrified SiSiC open cell foam was used as a resistive element to provide heat to Rh-based catalyst pellets packed inside the cells of the foam. A lab-scale reactor was tested in methane steam reforming conditions in a temperature range spanning from 600 to 800 °C providing encouraging results in a wide range of conditions. Full methane conversion was reached at sufficient high temperatures for GHSVs up to 15000 $NL/kg_{cat}/h$ and, at the same time, thermal efficiencies in excess of 70 %, power densities up to 10 MW/m^3 and specific energy consumptions of 1.33 kWh/Nm^3_{H2} were achieved in the lab-scale rig. A 2-D heterogeneous model of the electrified packed foam reactor was developed as a useful tool for designing scaled-up units. After validation against the experimental results, the model was used to simulate industrial units sized for different purposes. To comply simultaneously with the requirements of low pressure drops and high electric resistance, we proposed the strategy of sectioning the SiSiC foam. By cutting the cylindrical foam into several slices electrically connected in series, in fact, it is possible to decouple the aspect ratio (length/cross sectional area) of the electric circuit from the pneumatic one. This solution allows to design reactors characterized by low length/diameter ratios which guarantee limited pressure drops and, at the same time, satisfy the requirements on the electric resistance. Overall, we demonstrated the feasibility of realizing Joule heated packed foam reactors, a solution that aims at providing a more practical and reliable solution with respect to washcoated Joule heated reactors. We would like to point out that the use of packed foam reactors offers significant advantages in terms of reliability and possibility of increasing the catalyst inventory rather than in terms of pure performance indicators. In fact, packed foam reactors are not affected by issues related to catalyst erosion and to poor adhesion to the support, which are known drawbacks of solutions where catalyst is deposited on a surface.

With the electrified packed foam concept, we pave the way for the efficient electrification of packed bed reactors, providing a reliable and solid alternative also for other processes which require large catalyst

Table 3
Key performance indicators of the scaled-up units sized to produce 200 Nm^3/h of hydrogen.

Case [−]	N.sections [−]	Power [kW]	U [V]	I [A]	H_2fl.rate [Nm^3/h]	Tout [°C]	X_{CH4} [%]	Press. drop [bar]	Sp.Cons. [kWh/Nm^3_{H2}]
A	1	216	340	633	197	800	89	8	1.1
A	2	216	340	633	197	800	89	1.5	1.1
A	4	216	340	633	197	800	89	0.3	1.1
B	10	2000	1677	1193	1718	900	88.6	0.1	1.16

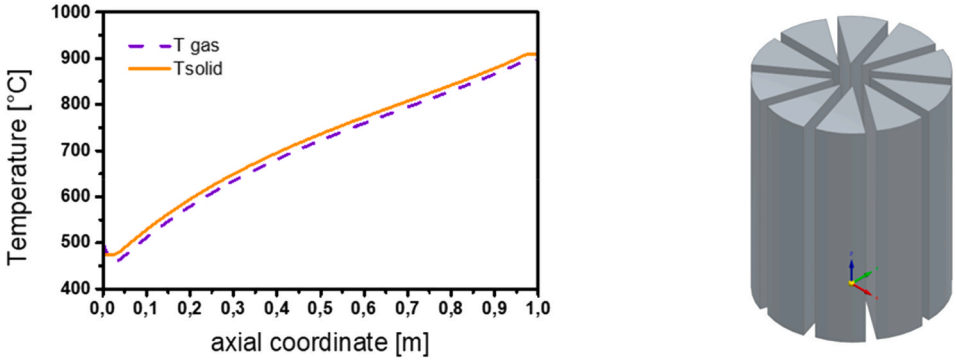

Fig. 14. Case B: industrial scale reactor (height = 1 m; diameter = 0.65 m) with nominal electric power of 2 MW. Simulated axial temperature profiles and reactor exploded view.

inventories and high working temperatures, such as ammonia cracking and Reverse Water Gas Shift.

CRediT authorship contribution statement

Federico Nicolini: Writing – original draft, Methodology, Investigation, Data curation, Conceptualization. **Matteo Ambrosetti:** Writing – review & editing, Methodology, Conceptualization. **Alessandra Beretta:** Writing – review & editing, Methodology, Conceptualization. **Gianpiero Groppi:** Writing – review & editing, Supervision, Methodology, Conceptualization. **Enrico Tronconi:** Writing – review & editing, Project administration, Funding acquisition, Conceptualization.

Declaration of competing interest

The authors declare that they have no known competing financial interests or personal relationships that could have appeared to influence the work reported in this paper.

Acknowledgment

Financial support from M.U.R. Progetti di Ricerca di Rilevante Interesse Nazionale (PRIN) Bando 2020 under the project 2020N38E75-"PLUG-IN" is gratefully acknowledged.

Appendix A. Supplementary data

Supplementary data to this article can be found online at https://doi.org/10.1016/j.ijhydene.2026.153393.

References

[1] Rogelj J, Popp A, Calvin KV, Luderer G, Emmerling J, Gernaat D, et al. Scenarios towards limiting global mean temperature increase below 1.5 °c. Nat Clim Change 2018;8:325–32. https://doi.org/10.1038/s41558-018-0091-3.
[2] Paltsev S, Morris J, Kheshgi H, Herzog H. Hard-to-Abate sectors: the role of industrial carbon capture and storage (CCS) in emission mitigation. Appl Energy 2021;300. https://doi.org/10.1016/j.apenergy.2021.117322.
[3] Gabrielli P, Rosa L, Gazzani M, Meys R, Bardow A, Mazzotti M, et al. Net-zero emissions chemical industry in a world of limited resources. One Earth 2023;6:682–704. https://doi.org/10.1016/j.oneear.2023.05.006.
[4] Woodall CM, Fan Z, Lou Y, Bhardwaj A, Khatri A, Agrawal M, et al. Technology options and policy design to facilitate decarbonization of chemical manufacturing. Joule 2022;6:2474–99. https://doi.org/10.1016/j.joule.2022.10.006.
[5] Meng F, Wagner A, Kremer AB, Kanazawa D, Leung JJ, Goult P, et al. Planet-compatible pathways for transitioning the chemical industry. Proc Natl Acad Sci U S A 2023;120. https://doi.org/10.1073/pnas.2218294120.
[6] Neuwirth M, Fleiter T, Manz P, Hofmann R. The future potential hydrogen demand in energy-intensive industries - a site-specific approach applied to Germany. Energy Convers Manag 2022;252. https://doi.org/10.1016/j.enconman.2021.115052.
[7] Azadnia AH, McDaid C, Andwari AM, Hosseini SE. Green hydrogen supply chain risk analysis: a european hard-to-abate sectors perspective. Renew Sustain Energy Rev 2023;182. https://doi.org/10.1016/j.rser.2023.113371.
[8] Apostolou D, Enevoldsen P, Xydis G. Supporting green urban mobility – the case of a small-scale autonomous hydrogen refuelling station. Int J Hydrogen Energy 2019;44:9675–89. https://doi.org/10.1016/j.ijhydene.2018.11.197.
[9] Muradov N. Low to near-zero CO2 production of hydrogen from fossil fuels: status and perspectives. Int J Hydrogen Energy 2017;42:14058–88. https://doi.org/10.1016/j.ijhydene.2017.04.101.
[10] Oni AO, Anaya K, Giwa T, Di Lullo G, Kumar A. Comparative assessment of blue hydrogen from steam methane reforming, autothermal reforming, and natural gas decomposition technologies for natural gas-producing regions. Energy Convers Manag 2022;254. https://doi.org/10.1016/j.enconman.2022.115245.
[11] van Geem KM, Galvita VV, Marin GB. Making chemicals with electricity. Science 2019;364:734–5. https://doi.org/10.1126/science.aax5179. 1979.
[12] Meloni E, Martino M, Palma V. Microwave assisted steam reforming in a high efficiency catalytic reactor. Renew Energy 2022;197:893–901. https://doi.org/10.1016/j.renene.2022.07.157.
[13] Hrabovsky M, Hlina M, Kopecky V, Maslani A, Krenek P, Serov A, et al. Steam plasma methane reforming for hydrogen production. Plasma Chem Plasma Process 2018;38:743–58. https://doi.org/10.1007/s11090-018-9891-5.
[14] Vinum MG, Almind MR, Engbæk JS, Vendelbo SB, Hansen MF, Frandsen C, et al. Dual-Function cobalt–nickel nanoparticles tailored for high-temperature induction-heated steam methane reforming. Angew Chem 2018;130:10729–33. https://doi.org/10.1002/ange.201804832.
[15] Zheng L, Ambrosetti M, Tronconi E. Joule-Heated catalytic reactors toward decarbonization and process intensification: a review. ACS Eng Au 2024;4:4–21. https://doi.org/10.1021/acsengineeringau.3c00045.
[16] Ambrosetti M. A perspective on power-to-heat in catalytic processes for decarbonization. Chem Eng Process Process Intensif 2022;182. https://doi.org/10.1016/j.cep.2022.109187.
[17] Wismann ST, Engbæk JS, Vendelbo SB, Bendixen FB, Eriksen WL, Aasberg-Petersen K, et al. Electrified methane reforming: a compact approach to greener industrial hydrogen production. Science 2019;364:756–9. https://doi.org/10.1126/science.aaw8775.
[18] Wismann ST, Engbæk JS, Vendelbo SB, Eriksen WL, Frandsen C, Mortensen PM, et al. Electrified methane reforming: elucidating transient phenomena. Chem Eng J 2021;425. https://doi.org/10.1016/j.cej.2021.131509.
[19] Balakotaiah V, Ratnakar RR. Modular reactors with electrical resistance heating for hydrocarbon cracking and other endothermic reactions. AIChE J 2022;68. https://doi.org/10.1002/aic.17542.
[20] Idamakanti M, Ledesma EB, Ratnakar RR, Harold MP, Balakotaiah V, Bollini P. Electrified catalysts for endothermic chemical processes: materials needs, advances, and challenges. ACS Eng Au 2024;4:71–90. https://doi.org/10.1021/acsengineeringau.3c00051.
[21] Pashchenko D, Papkov V. Steam methane reforming over a catalyst-coated wire with Joule heating: heat and mass transfer study in catalyst-wire system. Int J Hydrogen Energy 2025;170. https://doi.org/10.1016/j.ijhydene.2025.151164.
[22] Rieks M, Bellinghausen R, Kockmann N, Mleczko L. Experimental study of methane dry reforming in an electrically heated reactor. Int J Hydrogen Energy 2015;40:15940–51. https://doi.org/10.1016/j.ijhydene.2015.09.113.
[23] Mittal A, Ierapetritou M, Vlachos DG. Computational insights into steady-state and dynamic Joule-heated reactors. React Chem Eng 2024;9:2380–92. https://doi.org/10.1039/d4re00114a.
[24] Dong Q, Yao Y, Cheng S, Alexopoulos K, Gao J, Srinivas S, et al. Programmable heating and quenching for efficient thermochemical synthesis. Nature 2022;605:470–6. https://doi.org/10.1038/s41586-022-04568-6.
[25] Mortensen PM, Klein R, Aasberg-Petersen K. Inventors; TOPSOE A/S, applicant. Endothermic reactions heated by resistance heating. In: Patent application US 2021/0113983 A1; 2021.
[26] Pauletto G. inventor; Pauletto G. applicant. A reactor with an electrically heated structured ceramic catalyst. EU patent EP 3895795 A1, 2021.
[27] Kapteijn F, Moulijn JA. Structured catalysts and reactors – perspectives for demanding applications. Catal Today 2022;383:5–14. https://doi.org/10.1016/j.cattod.2020.09.026.

[28] Tronconi E, Groppi G, Visconti CG. Structured catalysts for non-adiabatic applications. Curr Opin Chem Eng 2014;5:55–67. https://doi.org/10.1016/j.coche.2014.04.003.
[29] Stankiewicz A, Moulijn JA. Process intensification. Ind Eng Chem Res 2002;41:1920–4. https://doi.org/10.1021/ie011025p.
[30] Bracconi M, Ambrosetti M, Maestri M, Groppi G, Tronconi E. A fundamental investigation of gas/solid mass transfer in open-cell foams using a combined experimental and CFD approach. Chem Eng J 2018;352:558–71. https://doi.org/10.1016/j.cej.2018.07.023.
[31] Zheng L, Ambrosetti M, Marangoni D, Beretta A, Groppi G, Tronconi E. Electrified methane steam reforming on a washcoated <scp>SiSiC</scp> foam for low-carbon hydrogen production. AIChE J 2023;69. https://doi.org/10.1002/aic.17620.
[32] Zheng L, Ambrosetti M, Beretta A, Groppi G, Tronconi E. Electrified CO2 valorization driven by direct Joule heating of catalytic cellular substrates. Chem Eng J 2023;466. https://doi.org/10.1016/j.cej.2023.143154.
[33] Zheng L, Ambrosetti M, Zaio F, Beretta A, Groppi G, Tronconi E. Direct electrification of Rh/Al2O3 washcoated SiSiC foams for methane steam reforming: an experimental and modelling study. Int J Hydrogen Energy 2023;48:14681–96. https://doi.org/10.1016/j.ijhydene.2022.12.346.
[34] Song X, Bao Z, Jiao Y. Numerical simulation of ethanol steam reforming on structured SiC foam catalyst with direct electrical heating. Fuel 2025;396. https://doi.org/10.1016/j.fuel.2025.135332.
[35] Zheng L, Wang D, Jiang Y, Ren Y, Wu Y, Fu Y, et al. Volumetric internal Joule heating of a catalyst packed SiSiC foam for efficient dry reforming of methane. Chem Eng J 2025;503. https://doi.org/10.1016/j.cej.2024.158291.
[36] Lu YR, Pudasainee D, Khan M, Gupta R, Nikrityuk PA. Experimental and Numerical study of volt–ampere characteristics of a packed tube heated by Joule heating. Journal of Energy Resources Technology, Transactions of the ASME 2022;144. https://doi.org/10.1115/1.4053303.
[37] Lu YR, Nikrityuk PA. Scale-up studies on electrically driven steam methane reforming. Fuel 2022;319. https://doi.org/10.1016/j.fuel.2022.123596.
[38] Turan E, Dieckmann R, Geske M, d'Alnoncourt RN, Bender M, Bode J, et al. Direct resistive heating of a catalytic fixed-bed reactor for ethanol dehydration. Chem Eng J 2025;514. https://doi.org/10.1016/j.cej.2025.162963.
[39] Agrawal R, West DH, Balakotaiah V. Modeling and analysis of local hot spot formation in down-flow adiabatic packed-bed reactors. Chem Eng Sci 2007;62:4926–43. https://doi.org/10.1016/j.ces.2006.11.057.
[40] Ambrosetti M, Bracconi M, Maestri M, Groppi G, Tronconi E. Packed foams for the intensification of catalytic processes: assessment of packing efficiency and pressure drop using a combined experimental and numerical approach. Chem Eng J 2020;382. https://doi.org/10.1016/j.cej.2019.122801.
[41] Ferri G, Ambrosetti M, Beretta A, Groppi G, Tronconi E, Agosti A. A novel electrified methane steam reformer for intensified H2 production based on conductive packed foams: experimental and modelling assessment. Chem Eng J 2025:168753. https://doi.org/10.1016/j.cej.2025.168753.
[42] Ambrosetti M, Bonincontro D, Balzarotti R, Beretta A, Groppi G, Tronconi E. H2 production by methane steam reforming over Rh/Al2O3 catalyst packed in Cu foams: a strategy for the kinetic investigation in concentrated conditions. Catal Today 2022;387:107–18. https://doi.org/10.1016/j.cattod.2021.06.003.
[43] NIST-JANAF. https://janaf.nist.gov/(accessed January 2024), 2024.
[44] Delgado JMPQ. Longitudinal and transverse dispersion in porous media. Chem Eng Res Des 2007;85:1245–52. https://doi.org/10.1205/cherd07017.
[45] Bracconi M, Ambrosetti M, Maestri M, Groppi G, Tronconi E. A fundamental analysis of the influence of the geometrical properties on the effective thermal conductivity of open-cell foams. Chem Eng Process Process Intensif 2018;129:181–9. https://doi.org/10.1016/j.cep.2018.04.018.
[46] Specchia V, Sicardi S. Modified correlation for the conductive contribution of thermal conductivity in packed bed reactors. Chem Eng Commun 1980;6:131–9. https://doi.org/10.1080/00986448008912525.
[47] Balzarotti R, Ambrosetti M, Beretta A, Groppi G, Tronconi E. Investigation of packed conductive foams as a novel reactor configuration for methane steam reforming. Chem Eng J 2020;391. https://doi.org/10.1016/j.cej.2019.123494.
[48] Ambrosetti M, Groppi G, Schwieger W, Tronconi E, Freund H. Packed periodic open cellular structures – an option for the intensification of non-adiabatic catalytic processes. Chem Eng Process Process Intensif 2020;155. https://doi.org/10.1016/j.cep.2020.108057.
[49] Ferri G, Ambrosetti M, Beretta A, Groppi G, Tronconi E. Experimental investigation and 2D mathematical modelling of copper foams packed with Rh-Al2O3 catalysts for the intensification of methane steam reforming. Catal Today 2024;426. https://doi.org/10.1016/j.cattod.2023.114386.
[50] Dixon AG. An improved equation for the overall heat transfer coefficient in packed beds. Chem Eng Process Process Intensif 1996;35:323–31. https://doi.org/10.1016/0255-2701(96)80012-2.
[51] Ambrosetti M, Beretta A, Groppi G, Tronconi E. A numerical investigation of electrically-heated methane steam reforming over structured catalysts. Frontiers in Chemical Engineering 2021;3. https://doi.org/10.3389/fceng.2021.747636.
[52] Aghaei P, Visconti CG, Groppi G, Tronconi E. Development of a heat transport model for open-cell metal foams with high cell densities. Chem Eng J 2017;321:432–46. https://doi.org/10.1016/j.cej.2017.03.112.
[53] Wismann ST, Engbæk JS, Vendelbo SB, Eriksen WL, Frandsen C, Mortensen PM, et al. Electrified methane reforming: understanding the dynamic interplay. Ind Eng Chem Res 2019;58:23380–8. https://doi.org/10.1021/acs.iecr.9b04182.
[54] Dong Y, Chen Z, Li X, Wang H, Han Z, Ma S, et al. Influence of power quality and stack temperature on the specific energy consumption of alkaline electrolyzer. IET Renew Power Gener 2024. https://doi.org/10.1049/rpg2.13007.
[55] From TN, Partoon B, Rautenbach M, Østberg M, Bentien A, Aasberg-Petersen K, et al. Electrified steam methane reforming of biogas for sustainable syngas manufacturing and next-generation of plant design: a pilot plant study. Chem Eng J 2024;479. https://doi.org/10.1016/j.cej.2023.147205.
[56] Sperle T, Chen D, Lødeng R, Holmen A. Pre-reforming of natural gas on a Ni catalyst. Criteria for carbon free operation. Appl Catal Gen 2005;282:195–204. https://doi.org/10.1016/j.apcata.2004.12.011.
[57] Hygear. https://hygear.com/technology/steam-methane-reforming/. [Accessed 18 July 2025].